MATHEMATICAL MODELING AND COMPUTING, Vol. 11, No. 3, pp. 642–653 (2024)

Total fractional-order variation and bilateral filter for image denoising

Addouch R.[1], Moussaid N.[1], Gouasnouane O.[1], Ben-Loghfyry A.[2]

[1]*LMCA, FSTM of Mohammedia, Hassan II University of Casablanca, Morocco*
[2]*LMCMAN, FSTM of Mohammedia, Hassan II University of Casablanca, Morocco*

(Received 8 December 2023; Revised 21 July 2024; Accepted 25 July 2024)

Image denoising stands out as a primary goal in image processing. However, many existing methods encounter challenges in preserving features such as corners and edges of an image while deleting the noise. This study investigates and evaluates a fractional-order derivative based on the total α-order variation (TV) model and the bilateral total variation (BTV) model. This choice is motivated by the proven effectiveness of the TV model in noise removal and edge preservation, with the BTV model further utilized to enhance the restoration of fine and intricate details. The experimental results affirm the efficacy of the proposed model, supported by objective quantitative metrics and subjective assessments of visual appearance.

Keywords: *image denoising; regularization; fractional-order derivatives; total α-order variation; bilateral total variation.*

2010 MSC: 65K10, 65N06, 74G30 **DOI:** 10.23939/mmc2024.03.642

1. Introduction

Image denoising constitutes a fundamental stage in digital image processing and computer vision, with the objective of eliminating or mitigating noise from a noisy image while retaining essential features and details. This noise can originate from diverse factors like sensor limitations, transmission errors, or environmental conditions. Frequently, it undermines the quality and utility of images across various applications, encompassing photography, medical imaging, surveillance, and more.

The general problem of image denoising can be formulated as follows:

$$\min_u \underbrace{\tfrac{1}{2}\|u-u_0\|_2^2}_{\text{fidelity term}} + \underbrace{\lambda R(u)}_{\text{Regularization term}},$$

$u = u(x)$ is the observed image, $x \in \Omega \subset \mathbb{R}^2$, Ω denotes the bounded domain of the image, u_0 is the initial image, and λ is a positive parameter representing a balance between the regularization and fidelity terms.

Over the years, researchers have proposed various regularization terms. The classical term $R(u) = \|\nabla u\|_2^2$ was introduced by Tikhonov and Arsenin and has achieved success. Unfortunately, this model falls short in preserving image edges. A more effective approach involves considering the total variation (TV) [1–5], where $R(u) = \int |Du|$. This formulation was proposed by Rudin, Osher, and Fatemi [6]:

$$\min_u \|u-u_0\|_2^2 + \mathrm{TV}(u).$$

The ROF model maintains the edges of the image by searching for solutions in the space of bounded variations BV functions. However, this model suffers from various limitations, such as the occurrence of the staircasing phenomenon and a decline in image contrasts. To recover a clear image, various methods have been devised to address imaging challenges such as image denoising [1, 7–11], image restoration [2, 3], image inpainting [12] and image super-resolution [4].

To overcome the aforementioned drawbacks, namely staircasing and contrast issues, the literature has introduced two alternative regularizers as substitutes for TV regularization. The first approach integrates higher-order regularization into image variational models. For example, Bredies, Kunish, and

Pock introduced the total generalized variation (TGV) regularizer. This involves a linear combination of higher-order derivatives and the total variation of u to effectively represent image denoising.

The second category introduces fractional-order derivatives [13–15]. As an illustration, Bai and Feng were the first to introduce fractional-order derivatives into anisotropic diffusion equations for noise removal,

$$\frac{\partial u}{\partial t} = -D_x^{\alpha *}\big(c(|D^\alpha u|)D^\alpha u\big) - D_y^{\alpha *}\big(c(|D^\alpha u|)D^\alpha u\big),$$

where $c(\cdot)$ represents the divergence parameter and $D_x^{\alpha *}$ represents the adjoint operator of D_x^α. For more models see [16–18].

The next interesting model was proposed by J. Zhang and K. Chen [3] based on the total fractional-order variation TV^α:

$$\min_u \frac{\lambda}{2}\,\|u - u_0\|_2^2 + \mathrm{TV}^\alpha(u).$$

These works have demonstrated the effectiveness of fractional-order derivatives in achieving a favorable balance, mitigating issues such as staircasing, and preserving crucial fine-scale features like edges and textures [1]. The latest interesting idea was a combination of the TV and the Bilateral Total Variation filter (BTV) (proposed in [5]):

$$\inf_{(u,k)} \left\{ F(u,k) := \|k * u - u_0\|_{L^2(\Omega)}^2 + \alpha_1\,\mathrm{BTV}(u) + \alpha_2\,\mathrm{TV}(k) \right\},$$

where $\alpha_1 > 0$ and $\alpha_2 > 0$ are two regularization parameters, k is the blur kernel and $*$ is the convolution operator.

The Bilateral Total Variation filter (BTV) is constructed by considering a larger neighborhood when computing the gradient at each pixel. This approach is designed to preserve sharp edges with less artefact. The BTV function is defined as follows:

$$\mathrm{BTV}(u) = \sum_{\substack{i=-p,\\ i\neq 0,1}}^{p} \sum_{\substack{j\neq -p,\\ j\neq 0,1}}^{p} \delta^{|i|+|j|} \left\| (I - S_x^i S_y^j)u \right\|_{L^1(\Omega)}.$$

In this expression, S_x^i and S_y^j denote two shift operators that shift the image u by i and j pixels in the horizontal and vertical directions, respectively, where $i + j > 0$. The parameter $\delta \in]0,1[$ is a scalar weight applied to introduce a spatially decaying effect to the summation of the regularization terms and the variable p represents the spatial window size.

2. Proposed model

Considering the inherent strengths and weaknesses of the previously mentioned regularization methods, we propose a novel approach that incorporates two distinct regularizers in the denoising process. These regularizers are the total fractional-order variation TV^α and the bilateral filter BTV. The integration of these two methods is motivated by the acknowledgment that the TV model effectively removes noise and preserves edges, while the BTV model excels in the precise restoration of intricate details. Thus, the formulation of our proposed model is as follows:

$$\min_u \left\{ F(u) = \frac{\lambda}{2}\,\|u - u_0\|_{L^2(\Omega)}^2 + \mathrm{TV}^\alpha(u) + \gamma\,\mathrm{BTV}(u) \right\},$$

where λ and γ are the regularization parameters and α represents the fractional order derivative with $1 < \alpha < 2$.

To substantiate the effectiveness of our proposed model, we employed the primal-dual algorithm and conducted extensive numerical experiments (for more details see [2, 17]).

3. Fractional derivatives

The fractional derivative serves as a generalization of the traditional derivative to non-integer orders. Several definitions exist, with the Grünwald–Letnikov (G-L), Riemann–Liouville (R-L), and Caputo definitions being among the most widely recognized. Among these, the G-L and R-L definitions stand out as the most popular choices employed in digital image processing.

The G-L definition is the next:

$$\text{G-L}\mathrm{D}^{\alpha}_{a,x} f(x) = \lim_{\substack{h\to 0 \\ Nh=x-a}} \left(\frac{1}{h}\right)^{\alpha} \sum_{i=0}^{N} (-1)^{\alpha} \binom{\alpha}{i} f(x-ih),$$

where the $\binom{\alpha}{j}$ are the binomial coefficients.

The R-L definition is:

$$\text{R-L}\mathrm{D}^{\alpha}_{a,x} f(x) = \frac{1}{\Gamma(n-\alpha)} \frac{d^n}{dx^n} \int_a^x \frac{1}{(x-s)^{\alpha+1-n}} f(s)\, ds \quad (n-1<\alpha<n),$$

where the $\Gamma(\cdot)$ is the gamma function, which is defined as:

$$\Gamma(n) = \int_0^{\infty} t^{n-1} e^{-t} dt.$$

The Caputo definition is:

$$\text{C}\mathrm{D}^{\alpha}_{a,x} f(x) = \frac{1}{\Gamma(n-\alpha)} \int_a^x \frac{1}{(x-s)^{\alpha+1-n}} f^n(s)\, ds \quad (n-1<\alpha<n).$$

In fact, the three definitions G-L, R-L and Caputo are equivalent under zero initial conditions.

Definition 1. *Let K denote the space of special test functions:*

$$K = \left\{ \phi \in \mathcal{C}_0^l(\Omega, \mathbb{R}^d), \text{ where } |\phi(x)| \leqslant 1, \text{ for all } x \in \Omega \right\},$$

where $|\phi(x)| = \sqrt{\sum_{i=1}^{d} \phi_i^2(x)}$, then the total α-order variation of u is defined by:

$$\mathrm{TV}^{\alpha}(u) = \int_{\Omega} |D^{\alpha} u| = \sup_{\phi \in K} \int_{\Omega} (-u \operatorname{div}^{\alpha} \phi)\, dx,$$

where $\operatorname{div}^{\alpha} \phi = \sum_{i=1}^{d} \frac{\partial^{\alpha} \phi_i}{\partial x_i^{\alpha}}$, the term $\frac{\partial^{\alpha} \phi_i}{\partial x_i^{\alpha}}$ represents a fractional α-order derivative of ϕ_i along the x_i direction.

Therefore, the space of functions with α-bounded variation on Ω is defined by:

$$\mathrm{BV}^{\alpha}(\Omega) = \left\{ u \in L^1(\Omega), \text{ where } \mathrm{TV}^{\alpha}(u) < +\infty \right\},$$

equipped with the BV-α norm:

$$\|u\|_{\mathrm{BV}^{\alpha}(\Omega)} = \|u\|_{L^1(\Omega)} + \mathrm{TV}^{\alpha}(u)$$

(for more details see [3]).

Lemma 1 (Lower semicontinuity). *Let be a sequence $\{v^k(x)\} \in \mathrm{BV}^{\alpha}(\Omega)$ such that $v^k(x) \underset{L^1(\Omega)}{\longrightarrow} v(x)$. Then $\mathrm{TV}^{\alpha}(v) \leqslant \liminf_{k\to\infty} \mathrm{TV}^{\alpha}(v^k)$.*

Proof. For the proof see [3]. ∎

Lemma 2. *The space $\mathrm{BV}^{\alpha}(\Omega)$ is a Banach space.*

Proof. For the proof see [3]. ∎

Definition 2 (a weak* topology). *The weak topology in $\mathrm{BV}^{\alpha}(\Omega)$ $\mathrm{BV}^{\alpha} - w^*$ is defined such as*

$$u_j \underset{\mathrm{BV}^{\alpha}-w^*}{\longrightarrow} u \Longleftrightarrow u_j \underset{L^1(\Omega)}{\longrightarrow} u \quad \text{and} \quad \int_{\Omega} \phi \cdot \nabla^{\alpha} u_j dx \longrightarrow \int_{\Omega} \phi \cdot \nabla^{\alpha} u\, dx$$

for all ϕ in $\mathcal{C}_0^1(\Omega, \mathbb{R}^d)$.

From this Definition, we can infer the weak compactness of $\mathrm{BV}^\alpha(\Omega)$ under the weak* topology. This, in conjunction with the weak lower semicontinuity of $F(u)$ and boundedness of Banach space $\mathrm{BV}^\alpha(\Omega)$, leads to the following result.

Theorem 1 (existence). *The functional $F(u)\colon \mathrm{BV}^\alpha(\Omega) \to \mathbb{R}$ has a minimum.*

Proof. The proof follows a similar rationale to the proof of [17, Prop. 38.12(d)]. ∎

Theorem 2 (uniqueness). *The functional $F(u)$ admits a unique solution in $\mathrm{BV}^\alpha(\Omega)$ when $\lambda > 0$.*

Proof. The convexity of the functional $F(u)$ leads to uniqueness of solutions. Refer to [17, Theorem 47C]. ∎

4. Discretization of the fractional derivative

Before introducing the finite difference discretization of the fractional derivative, we establish a spatial partition (x_k, y_l) (for all $k = 0, 1, \ldots, N+1$; $l = 0, 1, \ldots, M+1$) of the image domain Ω. We assume that u satisfies a zero Dirichlet boundary condition. We discretize the α-order fractional derivative along the x_i direction at the inner point (x_k, y_l), for all $k = 0, 1, \ldots, N$; $l = 0, 1, \ldots, M$ using the following approach

$$\begin{aligned} D^\alpha_{[a,b]}u(x_k, y_l) &= \frac{\delta^\alpha_0 u(x_k, y_l)}{h^\alpha} + O(h) = \frac{1}{2}\left(\frac{\delta^\alpha_- u(x_k, y_l)}{h^\alpha} + \frac{\delta^\alpha_+ u(x_k, y_l)}{h^\alpha}\right) + O(h) \\ &= \frac{1}{2}\left(h^{-\alpha}\sum_{j=0}^{k+1}\omega^\alpha_j u^l_{k-j+1} + h^{-\alpha}\sum_{j=0}^{N-k+2}\omega^\alpha_j u^l_{k+j-1}\right) + O(h), \end{aligned} \tag{1}$$

which is suitable for both the RL and C derivatives (see [11] and [16]). Where $u^l_s = u_{s,l}$, $\omega^{(\alpha)}_j = (-1)^j \binom{\alpha}{j}$, $j = 0, 1, \ldots, N+1$, and

$$\omega^{(\alpha)}_0 = 1; \quad \omega^{(\alpha)}_j = \left(1 - \frac{1+\alpha}{j}\right)\omega^{(\alpha)}_{j-1} \quad \text{for} \quad j > 0.$$

Upon examining (1), the estimation of the α-order fractional $D^\alpha_{[a,x]}u(x_k, y_l)$ along the x-direction at the point (x_k, y_l) with a fixed y_l involves a linear combination of $N+2$ values $\{u^l_0, u^l_1, \ldots, u^l_N, u^l_{N+1}\}$.

Incorporating the zero boundary condition into the matrix approximation of the fractional derivative, (1) can be simultaneously expressed in matrix form along the x direction:

$$\begin{pmatrix} \delta^\alpha u(x_1, y_l) \\ \delta^\alpha u(x_2, y_l) \\ \vdots \\ \vdots \\ \delta^\alpha u(x_N, y_l) \end{pmatrix} = \frac{1}{2}\begin{pmatrix} 2\omega^\alpha_1 & \omega & \omega^\alpha_3 & \ldots & \omega^\alpha_N \\ \omega & 2\omega^\alpha_1 & \ddots & \ddots & \vdots \\ \omega^\alpha_3 & \ddots & \ddots & \ddots & \omega^\alpha_3 \\ \vdots & \ddots & \ddots & 2\omega^\alpha_1 & \omega \\ \omega^\alpha_N & \ldots & \omega^\alpha_3 & \omega & 2\omega^\alpha_1 \end{pmatrix}\begin{pmatrix} u^l_1 \\ u^l_2 \\ \vdots \\ \vdots \\ u^l_N \end{pmatrix},$$

where $\omega = \omega^\alpha_0 + \omega^\alpha_2$.

The same procedure is applied to Ω along the y-direction.

5. Primal dual approach

The Primal Dual Projected Gradient (PDPG) algorithm is grounded in the Primal Dual approach, which converts the variational model into a saddle point problem through the application of the Legendre–Fenchel transform. Subsequently, numerous techniques have been introduced in the literature to resolve this saddle point problem. In our specific context, we employed the projected gradient method (for additional information, refer to [7]).

While U denotes the primal variable. We then obtain the following notations:

$$G(KU) := \sum_{k,l} |\nabla^\alpha U(k,l)|$$

and

$$F(U) := \sum_{k,l} \frac{\lambda}{2} \left(U(k,l) - U_0(k,l)\right)^2 + \gamma \sum_{n=-p}^{p} \sum_{m=-p}^{p} \delta^{|n|+|m|} \left|U(k,l) - S_x^n S_y^m U(k,l)\right|$$

with $V = \mathbb{R}^{n\times m}$ and $W = \mathbb{R}^{(n\times m)\times 2}$, V and W are two reflexive spaces. Next, we define the functionals:

$$\begin{aligned} K\colon V &\longrightarrow W \\ U &\longmapsto \nabla^\alpha U \end{aligned}$$

and

$$\begin{aligned} G\colon W &\longrightarrow \mathbb{R} \\ x &\longmapsto \sum_{k,l} g(x(k,l)), \end{aligned}$$

where

$$\begin{aligned} g\colon \mathbb{R}^2 &\longrightarrow \mathbb{R} \\ x &\longmapsto |x|. \end{aligned}$$

By using the definition of Legendre–Fenchel transform g^* of the function g, we define $g^*\colon \mathbb{R}^2 \to \mathbb{R}$ by:

$$g^*(s) = \begin{cases} 0 & \text{if } s \in [0,1], \\ +\infty & \text{otherwise.} \end{cases}$$

Hence, the convex conjugate G^* of G is:

$$\begin{aligned} G^*\colon W &\longrightarrow \mathbb{R} \\ \phi &\longmapsto \sum_{k,l} g^*(\phi(k,l)). \end{aligned}$$

Demonstrating the convexity of G is straightforward. Consequently, the equivalent Primal–Dual problem is expressed as:

$$\min_U \max_{\phi\in X} \left\{ \sum_{k,l} \langle \nabla^\alpha U, \phi\rangle + \frac{\lambda}{2}(U - U_0)^2 + \gamma \sum_{n=-p}^{p} \sum_{m=-p}^{p} \delta^{|n|+|m|} \left|U - S_x^n S_y^m U\right| \right\}, \tag{2}$$

where

$$X = W^* = \left\{\phi \in \mathbb{R}^{(n\times m)\times 2}, |\phi(k,l)|^2 \leqslant 1\right\}.$$

Considering that $1 \leqslant \alpha \leqslant 2$, we have $(\nabla^\alpha)^* = \operatorname{div}^\alpha$, the equation (2) can be reformulated as:

$$\min_U \max_{\phi\in X} \left\{ \sum_{k,l} U \operatorname{div}^\alpha \phi + \frac{\lambda}{2}(U - U_0)^2 + \gamma \sum_{n=-p}^{p} \sum_{m=-p}^{p} \delta^{|n|+|m|} \left|U - S_x^n S_y^m U\right| \right\}.$$

Next, we implement the projected gradient method. For every pair (k,l):

$$H(U,\phi) = \begin{pmatrix} \operatorname{div}^\alpha \phi + \lambda(U - U_0) + \gamma \sum\limits_{n=-p}^{p} \sum\limits_{m=-p}^{p} \delta^{|n|+|m|} \left(I - S_x^n S_y^m\right) \operatorname{sign}\left(U - S_x^n S_y^m U\right) \\ -\nabla^\alpha U \end{pmatrix}.$$

At an iteration i, we estimate (U^i, ϕ^i) using the projection algorithm at (k,l) by the following formula:

1) $\phi^{i+1} = P_X\left(\phi^i - r_1 \nabla^\alpha U^i\right)$,
2) $U^{i+1} = U^i - r_2 \Bigg(\operatorname{div}^\alpha \phi^{i+1} + \lambda(U^i - U_0)\gamma \sum\limits_{n=-p}^{p} \sum\limits_{m=-p}^{p} \delta^{|n|+|m|} (I - S_x^n S_y^m) \operatorname{sign}\left(U - S_x^n S_y^m U\right) \Bigg)$,

where r_1 and r_2 are two positive constants, and the projection P_X is defined by:

$$P_X(\phi)(l,k) = \frac{\phi(l,k)}{\max(1, |\phi(l,k)|)}.$$

Concludingly, we present a summary of the PDPG algorithm applied to our fractional image denoising model.

Algorithm 1 $\mathrm{TV}^\alpha - \mathrm{BTV}$ Denoising Model Enhanced by PDPG Algorithm.

1: **Inputs:** λ, δ (regularization parameters);
α (fractional-order derivative);
r_1, r_2 (fixed-point parameters);
U_0 (initial image);
ϕ^0 (the initial dual variable);

2: **Initialize:** $U^0 = U_0$;
$\phi^0 = 0$;

3: **repeat:**
$$\begin{cases} \bar{\phi}^{i+1} \leftarrow \phi^i - r_1 \nabla^\alpha U^i; \\ \phi^{i+1} \leftarrow \dfrac{\bar{\phi}^{i+1}}{\max\left(|\bar{\phi}^{i+1}|, 1\right)}; \\ U^{i+1} \leftarrow (1 - 2\lambda r_2) U^i - r_2 \Big(\operatorname{div}^\alpha \phi^{i+1} - 2\lambda U_0 \\ \quad + \gamma \sum_{n=-p}^{p} \sum_{m=-p}^{p} \delta^{|n|+|m|} (I - S_x^n S_y^m) \operatorname{sign}(U - S_x^n S_y^m U) \Big); \end{cases}$$

4: **until** convergence;

6. Numerical results

In this section we present some numerical results from using the Primal–Dual algorithm as an optimization method for the purpose of comparison. We compare our approach with the "Total Variation" (TV) and "Fractional Total Variation" (TV^α) models. To compare the performance of our method with the others, we used the "peak-signal-to-noise ratio" (PSNR) and the "mean structure similarity" (SSIM). In our initial set of experiments, we employ six images that have been corrupted by Gaussian noise.

In Figure 1 we present results for denoising a series of test images using $\lambda = 0.5$, $\alpha = 1.6$, $r1 = 0.95$, $r2 = 1.2$, $p = 6$, $\delta = 10^{-4}$ and $\gamma = 10^{-3}$. The images have been degraded by an additive Gaussian noise of standard deviation $\sigma = 10$.

In Table 1 we compare the restoration quality (via PSNR and SSIM) of six images. We can see that our approach shows a slight improvement compared to the other models.

In Figures 2–6 we proposed a high level of noise $\sigma = 20$ with different images.

Table 1. Comparisons between our approach with TV and TV^α models using the psnr(p) and ssim(s) values.

Original image	TV	TV^α	Our approach
Lena	$p = 30.42$	$p = 30.86$	$p = 30.90$
	$s = 0.888$	$s = 0.895$	$s = 0.900$
Peppers	$p = 30.74$	$p = 31.48$	$p = 31.50$
	$s = 0.878$	$s = 0.893$	$s = 0.894$
Geometric	$p = 31.06$	$p = 31.29$	$p = 31.33$
	$s = 0.743$	$s = 0.747$	$s = 0.748$
Satellite	$p = 30.94$	$p = 31.27$	$p = 31.32$
	$s = 0.622$	$s = 0.627$	$s = 0.628$
Brain	$p = 30.81$	$p = 31.11$	$p = 31.17$
	$s = 0.728$	$s = 0.730$	$s = 0.732$
Butterfly	$p = 30.50$	$p = 30.89$	$p = 30.93$
	$s = 0.902$	$s = 0.909$	$s = 0.911$

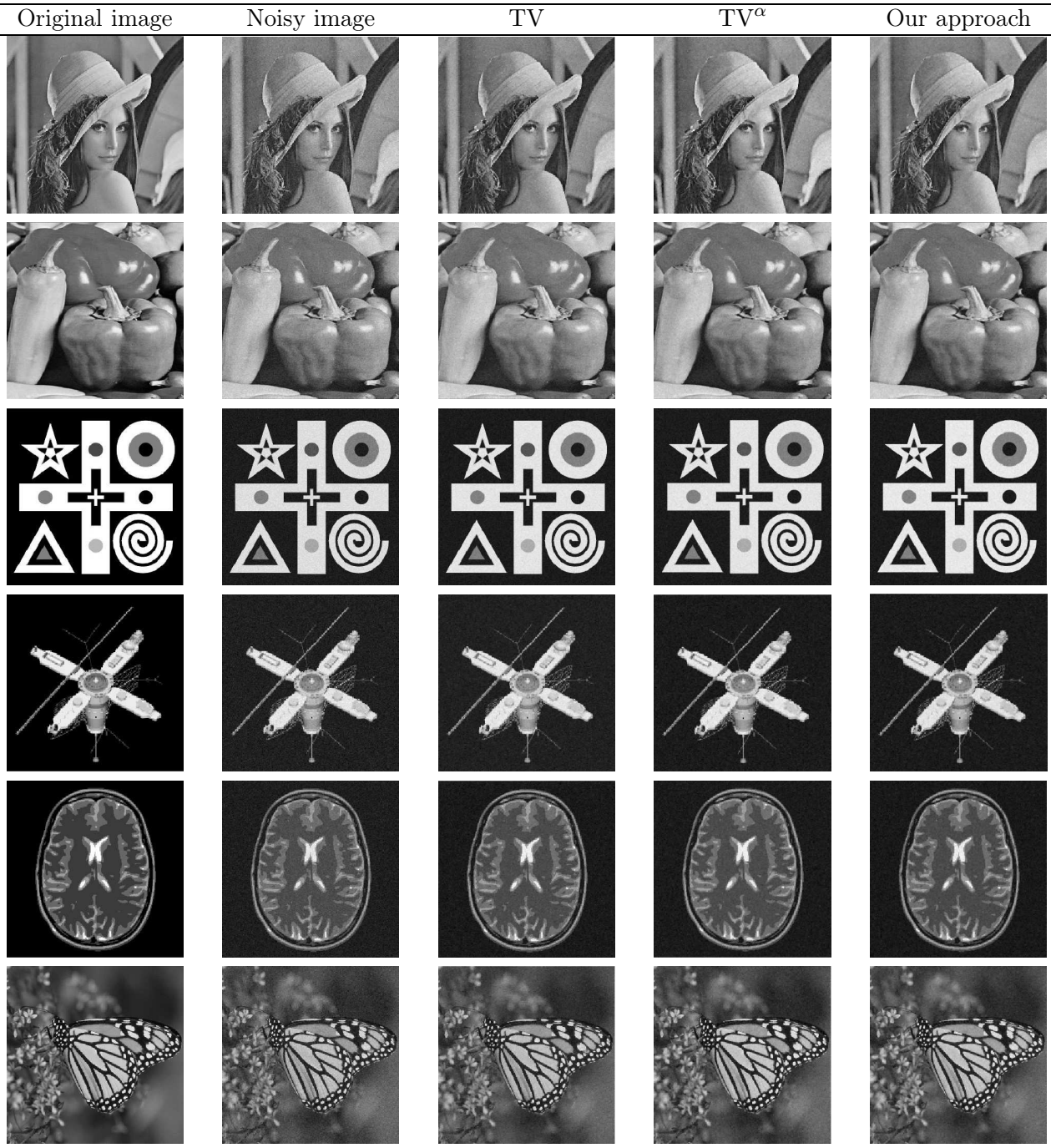

Fig. 1. Comparisons between our approach with TV and TV$^{\alpha}$ models.

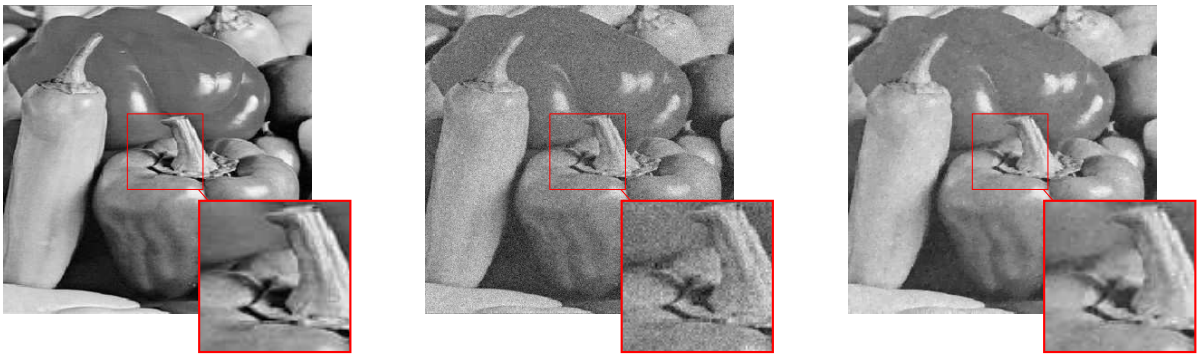

a (Reference image) ***b*** (Noisy image $\sigma = 20$) ***c*** (TV)

d (TV$^{\alpha}$) ***e*** (Our approach)

Fig. 2. Our approach vs. other models using Peppers image with $\sigma = 20$.

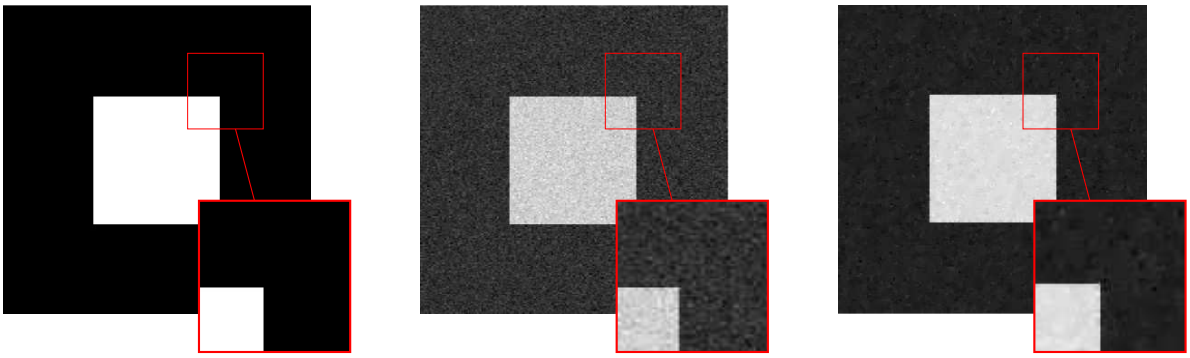

a (Reference image) ***b*** (Noisy image $\sigma = 20$) ***c*** (TV)

d (TV$^{\alpha}$) ***e*** (Our approach)

Fig. 3. Our approach vs. other models using Square image with $\sigma = 20$.

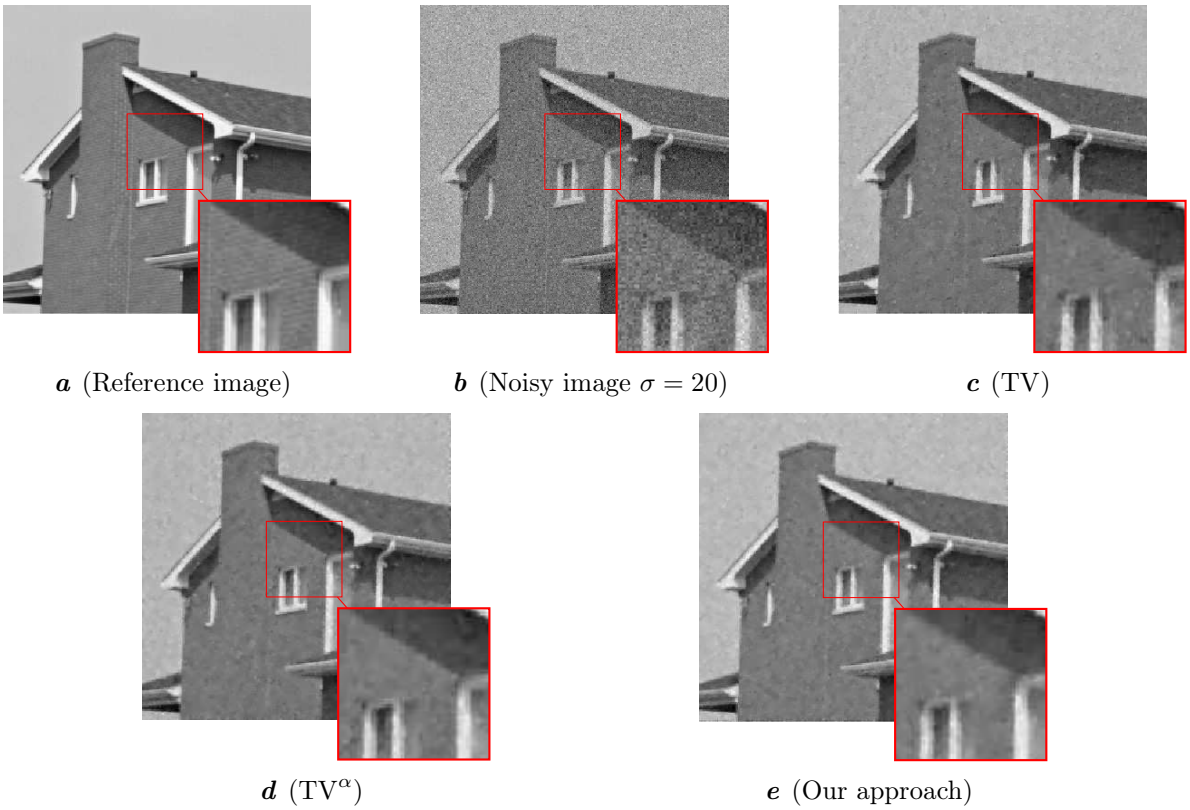

a (Reference image) ***b*** (Noisy image $\sigma = 20$) ***c*** (TV)

d (TV^{α}) ***e*** (Our approach)

Fig. 4. Our approach vs. other models using House image with $\sigma = 20$.

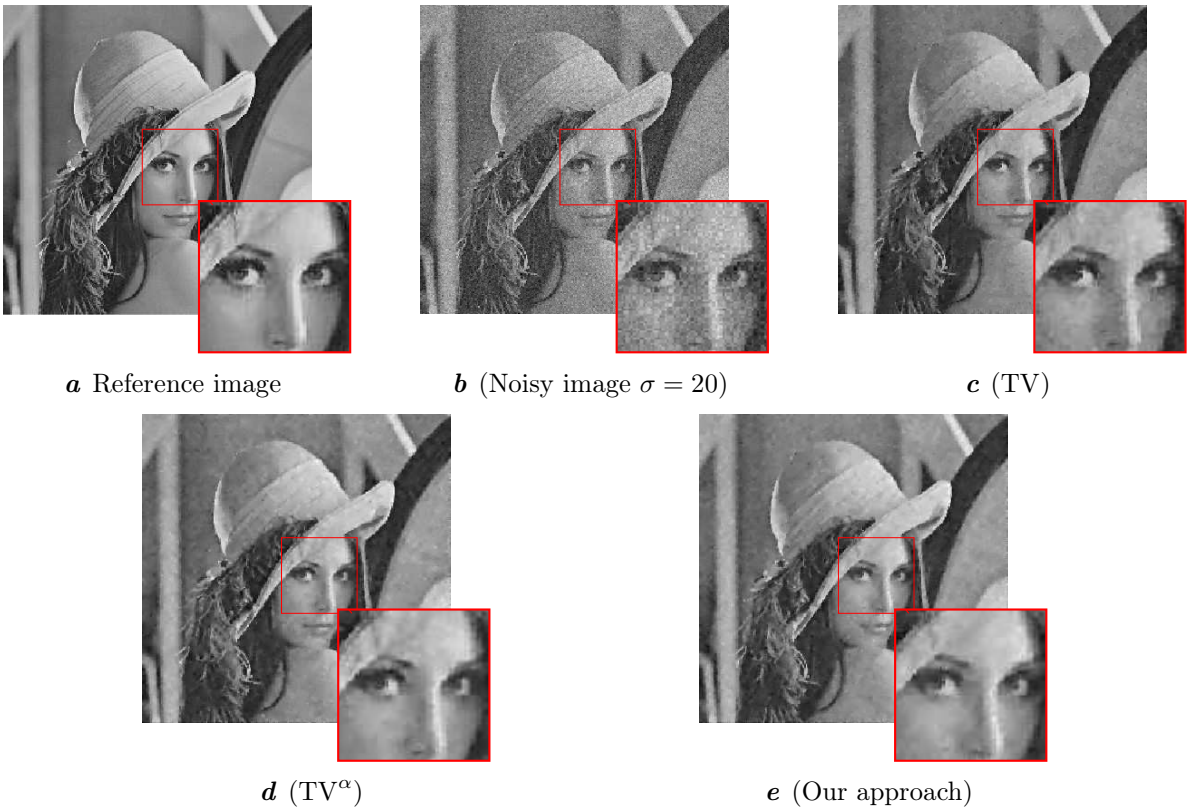

a Reference image ***b*** (Noisy image $\sigma = 20$) ***c*** (TV)

d (TV^{α}) ***e*** (Our approach)

Fig. 5. Our approach vs. Other models using Lena image with $\sigma = 20$.

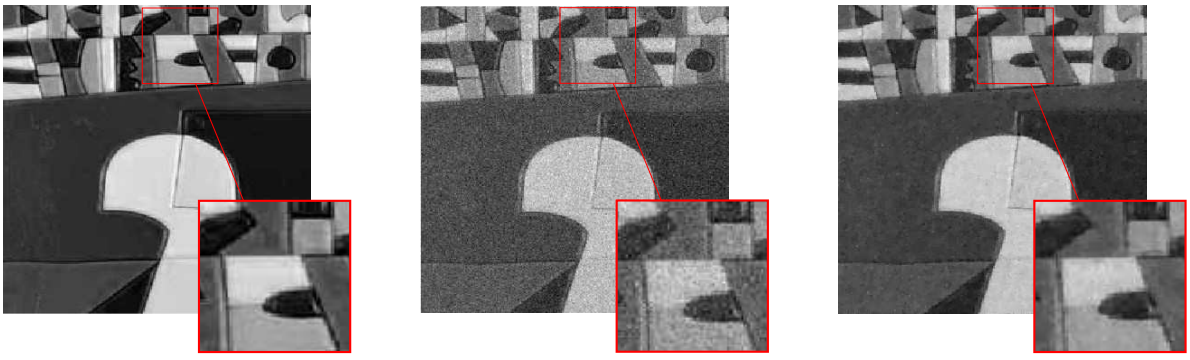

a Reference image ***b*** (Noisy image $\sigma = 20$) ***c*** (TV)

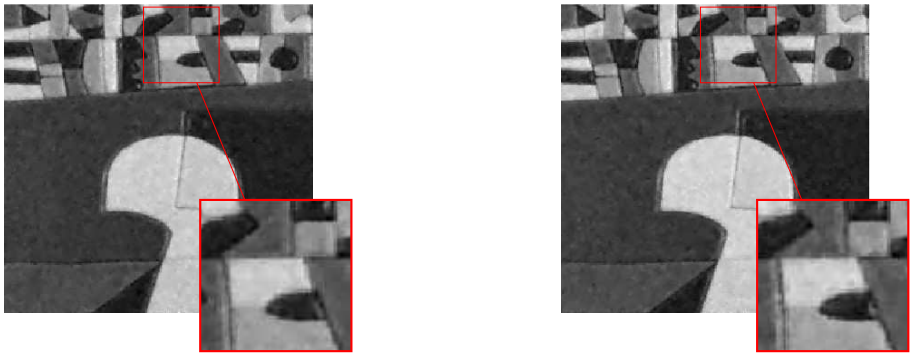

d (TV$^{\alpha}$) ***e*** (Our approach)

Fig. 6. Our approach vs. Other models using Paint image with $\sigma = 20$.

Table 2. The PSNR and SSIM values with a noise variance $\sigma = 20$.

Original image	TV	TV$^{\alpha}$	Our approach
Peppers	$p = 29.11$	$p = 30.15$	$p = 30.24$
	$s = 0.868$	$s = 0.903$	$s = 0.905$
House	$p = 29.20$	$p = 29.78$	$p = 29.87$
	$s = 0.867$	$s = 0.893$	$s = 0.894$
Lena	$p = 27.95$	$p = 27.99$	$p = 28.03$
	$s = 0.872$	$s = 0.892$	$s = 0.893$
Square	$p = 31.95$	$p = 32.62$	$p = 32.71$
	$s = 0.594$	$s = 0.599$	$s = 0.602$
Paint	$p = 29.05$	$p = 29.58$	$p = 29.67$
	$s = 0.875$	$s = 0.908$	$s = 0.908$

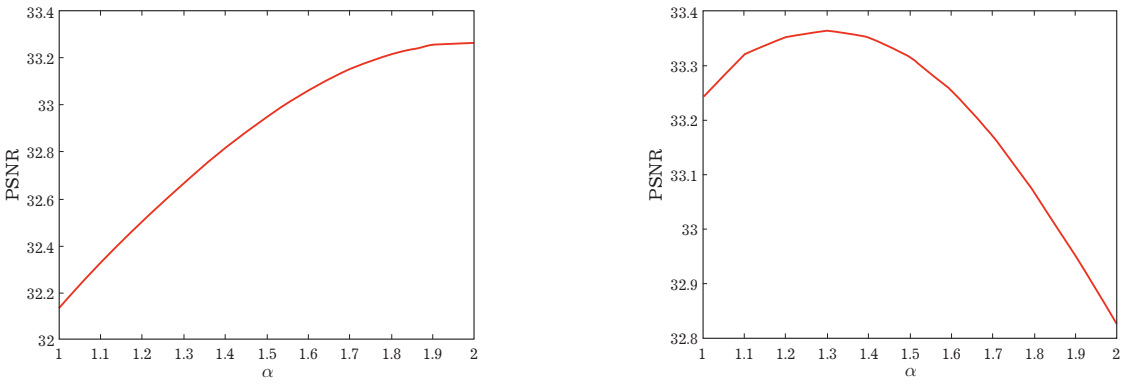

a (PSNR(α) with $\lambda = 0.1$) ***b*** (PSNR(α) with $\lambda = 0.005$)

Fig. 7. Sensitivity test of our approach to parameter λ with fixed $\sigma = 10$ for the Peppers image.

7. Conclusion

In this paper, we successfully integrate two significant and effective regularization terms for image noise removal. Our approach leverages the power of the fractional derivative total variation and the bilateral filter, both of which prove to be adept at preserving details while deleting noise. The efficacy of the fractional derivative tool in image denoising not only underscores its practicality but also paves the way for further exploration by researchers into additional models based on fractional calculus.

[1] Ben-Loghfyry A., Hakim A. A total variable-order variation model for image denoising. AIMS Mathematics. **4** (5), 1320–1335 (2019).

[2] Zhu M., Wright S. J., Chan T. F. Duality-based algorithms for total-variation-regularized image restoration. Computational Optimization and Applications. **47** (3), 377–400 (2010).

[3] Zhang J., Chen K. A Total fractional-order variation model for Image restoration with nonhomogeneous boundary conditions and its numerical solution. SIAM Journal on Imaging Sciences. **8** (4), 2487–2518 (2015).

[4] Laghrib A., Hakim A., Raghay S. A combined total variation and bilateral filter approach for image robust super resolution. EURASIP Journal on Image and Video Processing. **2015**, 19 (2015).

[5] El Mourabit I., El Rhabi M., Hakim A. Blind deconvolution using bilateral total variation regularization: a theoretical study and application. Applicable Analysis. **101** (16), 5660–5673 (2022).

[6] Rudin L. I., Osher S., Fatemi E. Nonlinear total variation based noise removal algorithms. Physica D: Nonlinear Phenomena. **60** (1–4), 259–268 (1992).

[7] Ben-Loghfyry A., Hakim A., Laghrib A. A denoising model based on the fractional Beltrami regularization and its numerical solution. Journal of Applied Mathematics and Computing. **69** (2), 1431–1463 (2023).

[8] Ben-Loghfyry A., Hakim A. Time-fractional difusion equation for signal and image smoothing. Mathematical Modeling and Computing. **9** (2), 351–364 (2022).

[9] Ben-Loghfyry A., Hakim A. Robust-time-fractional diffusion filtering for noise removal. Mathematical Methods in the Applied Sciences. **45** (16), 9719–9735 (2022).

[10] Ben-Loghfyry A., Charkaoui A. Regularized Perona & Malik model involving Caputo time-fractional derivative with application to image denoising. Chaos, Solitons & Fractals. **175** (1), 113925 (2023).

[11] Gouasnouane O., Moussaid N., Boujena S. A nonlinear fractional partial equation differential for image denoising. 2021 Third International Conference on Transportation and Smart Technologies (TST), Tangier, Morocco. 59–64 (2021).

[12] Gouasnouane O., Moussaid N., Boujena S., Kabli K. A nonlinear fractional partial differential equation for image inpainting. Mathematical Modeling and Computing. **9** (3), 536–546 (2022).

[13] Yang Q., Chen D., Zhao T., Chen Y. Fractional Calculus in Image Processing: A Review. Fractional Calculus and Applied Analysis. **19** (5), 1222–1249 (2016).

[14] Podlubny I., Chechkin A., Skovranek T., Chen Y., Vinagre-Jara B.M. Matrix approach to discrete fractional calculus II: Partial fractional differential equations. Journal of Computational Physics. **228** (1), 3137–3153 (2009).

[15] Wang H., Du N. Fast solution methods for space-fractional diffusion equations. Journal of Computational and Applied Mathematics. **255**, 376–383 (2014).

[16] Sayah A., Moussaid N., Gouasnouane O. Finite difference method for Perona-Malik model with fractional derivative and its application in image processing. 2021 Third International Conference on Transportation and Smart Technologies (TST), Tangier, Morocco. 101–106 (2021).

[17] Zosso D., Bustin R. A Primal-Dual Projected Gradient algorithm for efficient Beltrami regularization. UCLA CAM Report. 14–52 (2014).

[18] Zeidler E. Nonlinear functional analysis and its Applications. III. Variational methods and optimization. Springer-Verlag, New York (1985).

Загальна варіація дробового порядку та двосторонній фільтр для зменшення шуму зображення

Аддуш Р.[1], Муссаід Н.[1], Гуаснуан О.[1], Бен-Логфірі А.[2]

[1]*LMCA, FSTM Мохаммедії, Університет Хасана II Касабланки, Марокко*
[2]*LMCMAN, FSTM Мохаммедії, Університет Хасана II Касабланки, Марокко*

Усунення шумів на зображенні є основною метою обробки зображень. Однак багато існуючих методів стикаються з проблемами збереження таких особливостей, як кути та краї зображення, одночасно видаляючи шум. У статті досліджується та оцінюється похідна дробового порядку на основі моделі варіації загального α-порядку (TV) і моделі двосторонньої загальної варіації (BTV). Цей вибір обумовлений доведеною ефективністю моделі TV у видаленні шумів і збереженні країв, а модель BTV додатково використовується для покращення відновлення дрібних і складних деталей. Експериментальні результати підтверджують ефективність запропонованої моделі, що підтверджується об'єктивними кількісними показниками та суб'єктивними оцінками візуального вигляду.

Ключові слова: *зменшення шуму зображення; регулярізація; похідні дробового порядку; загальна варіація α-порядку; двостороння тотальна варіація.*